Supporting information

Selective Single Molecule Nanopore Sensing of microRNA Using PNA Functionalized Magnetic Core-shell Fe_3O_4-Au Nanoparticles

Hao Wang, Haoran Tang, Cheng Yang, Yongxin Li*

Anhui Key Laboratory of Chemo/Biosensing, College of Chemistry and Materials Science, Anhui Normal University, Wuhu, 241000, P.R. China

*corresponding author. Email: yongli@mail.ahnu.edu.cn

Phone: 86-553-386-9302; Fax: 86-553-386-9303

Contents

Table S1: Technical parameter of nanopores production.

	HEAT	FIL	VEL	DEL	PUL
Step 1	650	3	35	185	45
Step 2	900	3	15	128	200

Table S2: Zeta potential of different nanoparticles.

	Zeta potential (pH = 7.4)
Fe_3O_4-Au NP	-0.09 ± 0.04 mV
Fe_3O_4-Au-PNA	-0.12 ± 0.04 mV
Fe_3O_4-Au-PNA-RNA	-16.4 ± 1.8 mV

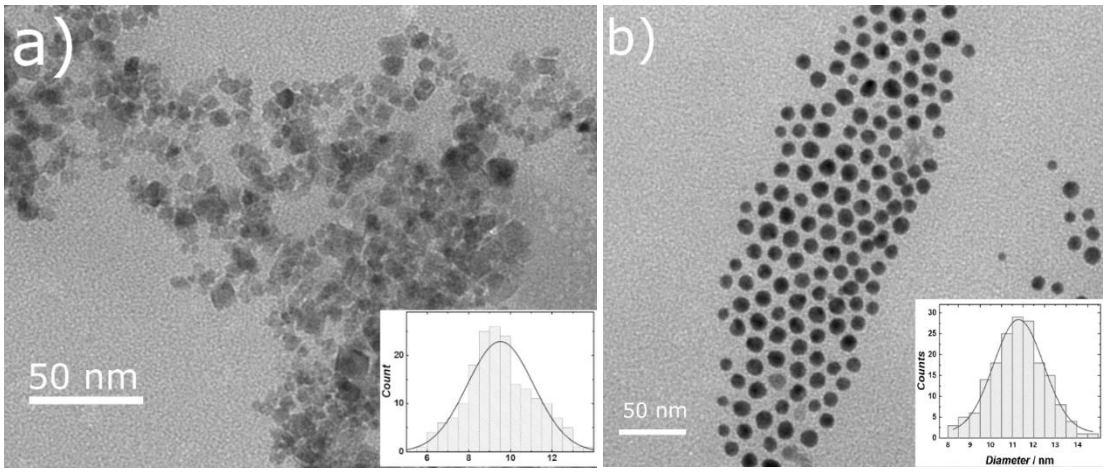

Figure S1. TEM images of the synthesized NPs: (a) parent Fe_3O_4 NPs; (b) core-shell Fe_3O_4-Au NPs.

In **Figure S1** are presented the TEM images of the Fe_3O_4 NPs and core-shell Fe_3O_4-Au NPs as well as the particle size distribution histograms. As can be observed from Figure S1 (a), the parent Fe_3O_4 NPs sample is composed of nanometer-sized particles with an average particle size of 9.2 ± 1.8 nm and a Gaussian-type size distribution. Upon the coating of Fe_3O_4 with gold, the presence of quasi-spherical nanoparticles with a darker contrast can be observed, as well as an increase of the particle size to 11.2 ± 1.6 nm, which confirms the successful formation of core-shell nanoparticles; furthermore, the nanoparticles are well-dispersed with no signs of aggregation and no free iron oxide cores are detected, indicating the complete encapsulation of the Fe_3O_4 cores.

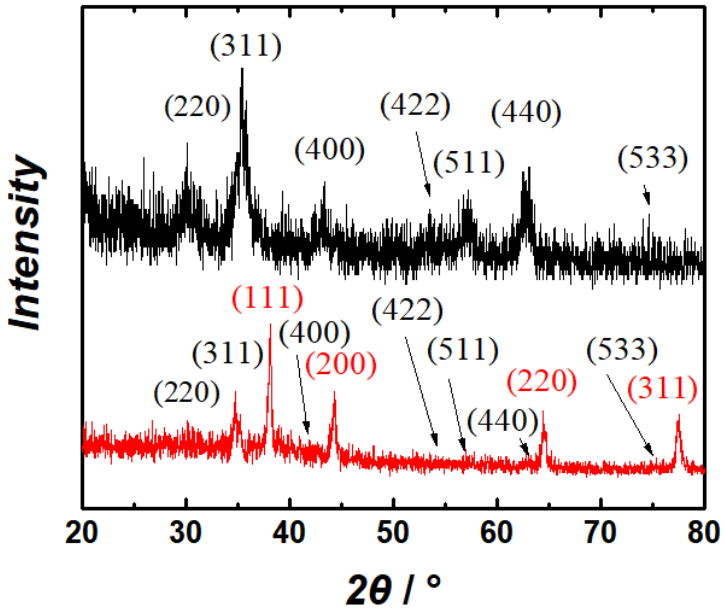

Figure S2. X-ray diffractograms of Fe_3O_4 (black) and Fe_3O_4-Au (red) samples.

In **Figure S2** are the diffractograms of the Fe_3O_4 (a) and core-shell Fe_3O_4-Au (b) NPs. The diffractogram of the parent Fe_3O_4 NPs presents the characteristic Bragg reflections of ferrites, (220), (311), (400), (422), (511), (440), and (533), revealing the crystalline nature of the nanomaterial and the cubic spinel structure.[1] Compared with the structure reported before, the XRD indicates that Fe_3O_4 was successfully prepared.[2] In the diffractogram of the core-shell Fe_3O_4-Au sample are detected additional diffraction peaks that can be indexed to the (111), (200), (220), and (311) planes of gold with a cubic structure, indicating its presence in the sample.[1] Furthermore, a decrease of the intensity of the Bragg reflections associated with magnetite is observed, which confirms the successful coating of the Fe_3O_4 cores with gold.

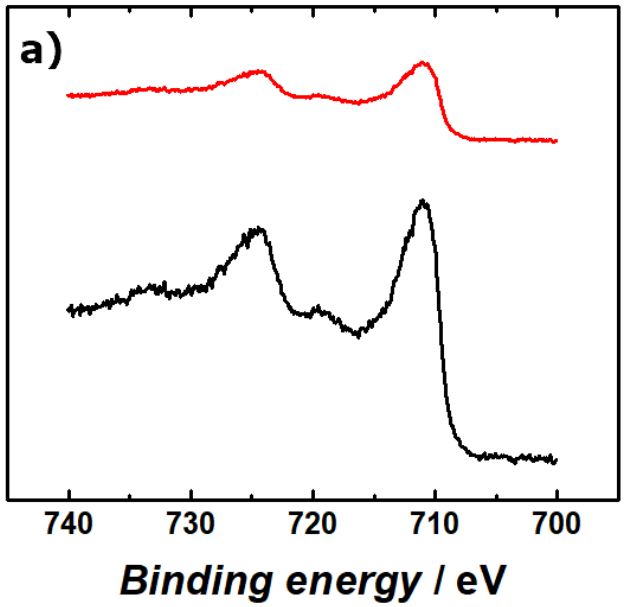
a)
740
730
720
710
700
Binding energy / eV

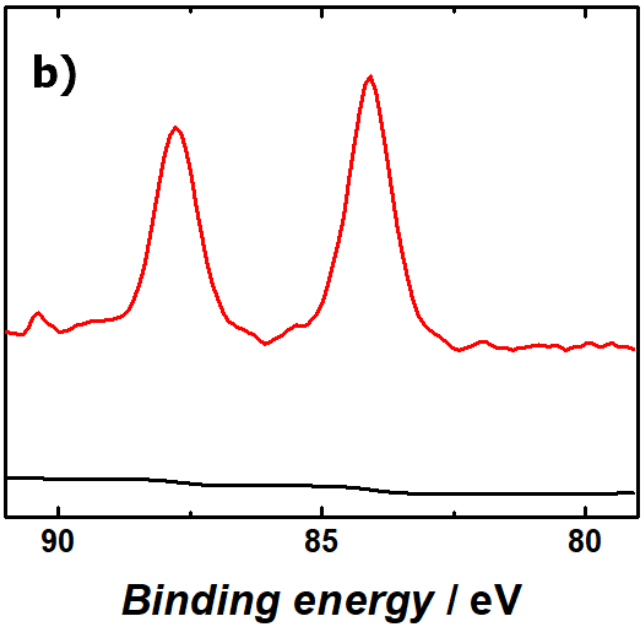
b)
90
85
80
Binding energy / eV

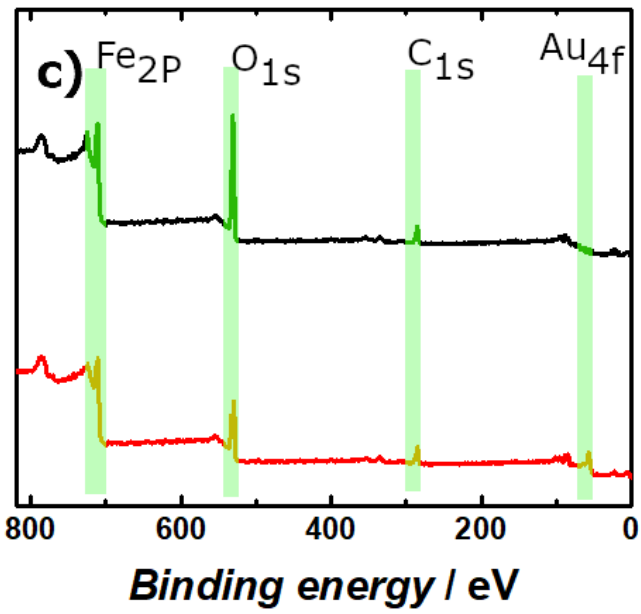

Figure S3. (a) Fe2p of Fe_3O_4 (black) and Fe_3O_4-Au (red), (b) Au4f of Fe_3O_4 (a) and Fe_3O_4-Au(red). (c). XPS spectra of Fe_3O_4 (black) and Fe_3O_4-Au (red).

XPS was further employed to compare the two interfaces of Fe_3O_4 (black) and Fe_3O_4-Au (red) nanocomposites. As shown in **Figure S3** (a), the groups at 726.5 eV and 710.3 eV correspond to $Fe2p_{1/2}$ and $Fe2p_{3/2}$, respectively. In Figure S3 (b), the peak doublet appearing at 83.7 eV ($Au4f_{7/2}$) and 86.9 eV ($Au4f_{5/2}$) is assigned to Au^0, while no peaks in Fe_3O_4 (black) are seen. This conclusion was also supported by full XPS spectra, both Fe_3O_4 (black) and Fe_3O_4-Au (red) present distinct peaks at 726.5 eV, 710.3 eV and 528.9 eV, which are attributed to $Fe2p_{1/2}$, $Fe2p_{3/2}$ and O1s, respectively.[3]

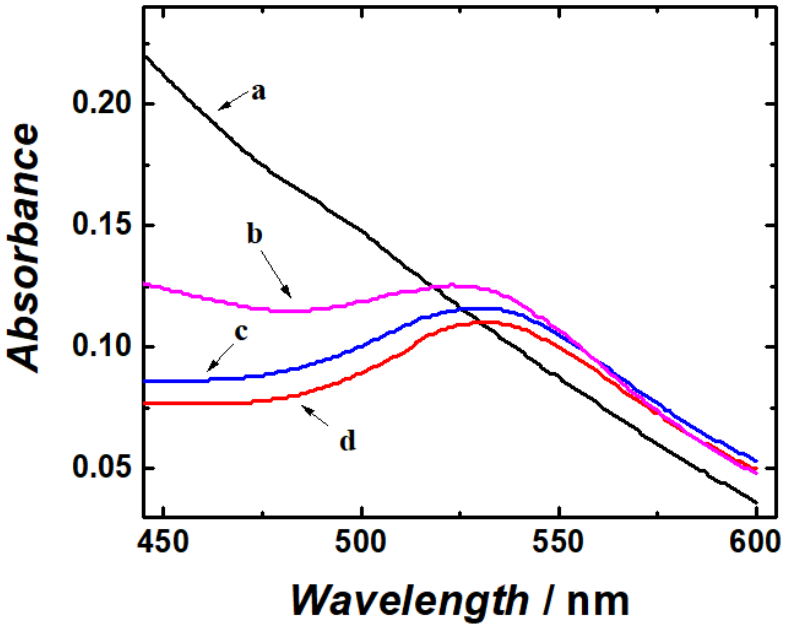

Figure S4. UV−vis spectra of bare Fe_3O_4 NPs (a), Fe_3O_4-Au NPs (b), Fe_3O_4-Au-PNA (c) and Fe_3O_4-Au-PNA-RNA (d).

The UV−vis spectra (**Figure S4**) of the bare Fe_3O_4 NPs dispersed in double distilled water showed the absence of any absorption band, which rules out the presence of free Au (curve a). In contrast, the spectrum of the Fe_3O_4-Au NPs, Fe_3O_4-Au-PNA and Fe_3O_4-Au-PNA-RNA exhibited the expected surface plasmon resonance band (SPR) centered at λ = 527 nm, 530 nm and 531 nm (curve b, c, d), respectively. This red shift of the SPR absorption band ongoing is due to the increase of the volume caused by the binding of PNA and RNA.

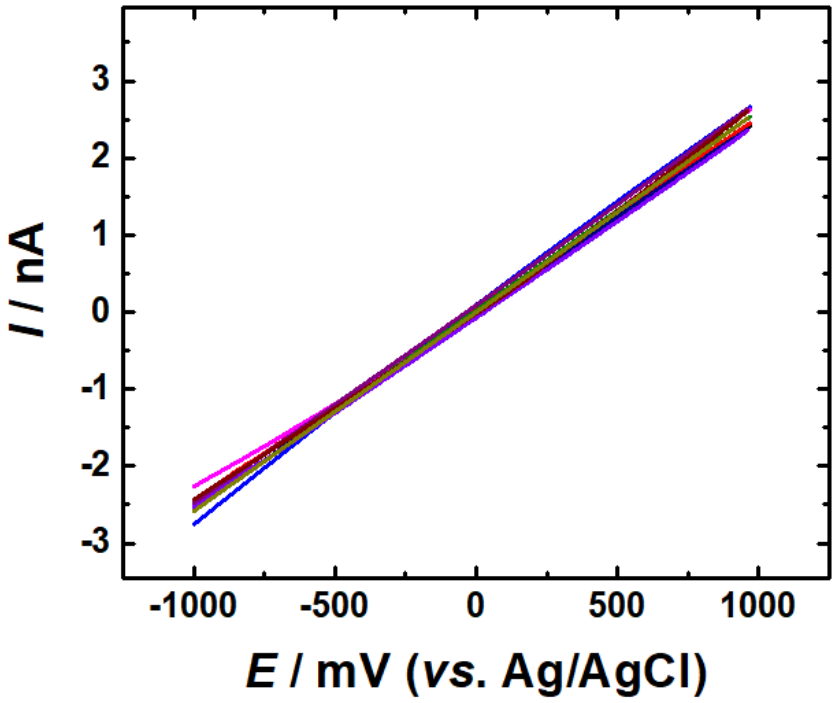

Figure S5. Current-voltage curves of 10 representative nanopipettes using 100 mM KCl, exhibiting current rectification behavior with a resistance of 336.2 ± 23 MΩ as measured in (-1 V, 1 V) regime. The nanopipettes used in this work had resistance variation within 7%.

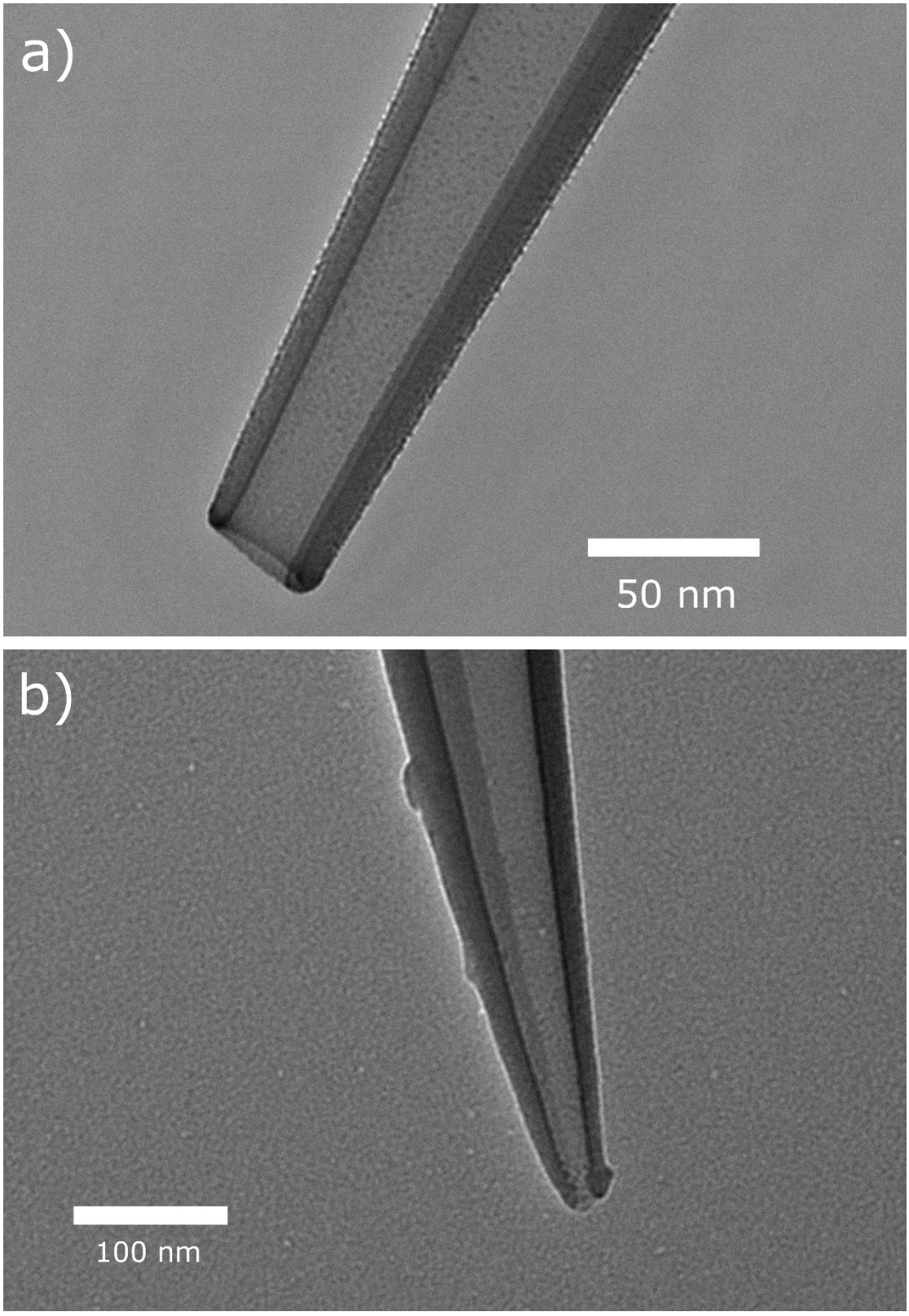
a)
50 nm
b)
100 nm

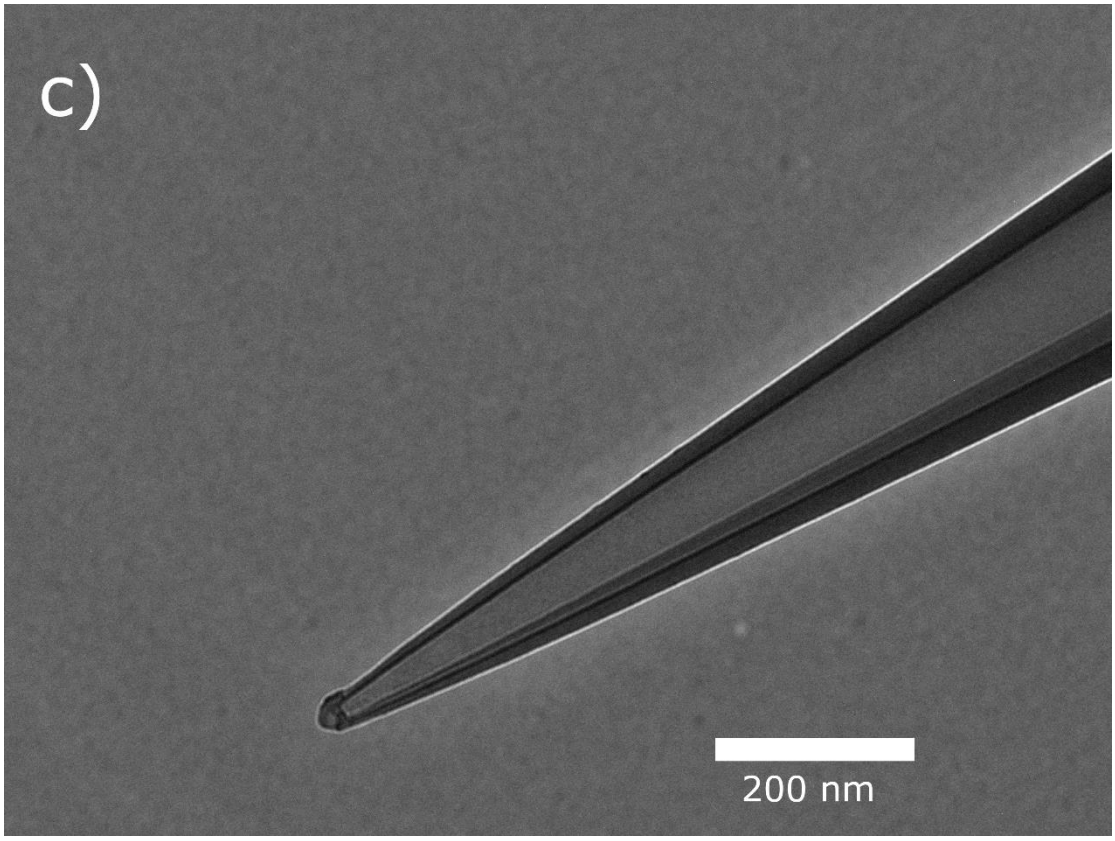

Figure S6. TEM images of different nanopores: a) 23.5 nm in diameter with a scale bar of 50 nm; b) 17.0 nm in diameter with a scale bar of 100 nm; c) 21.4 nm in dameter with a scale bar of 200 nm.

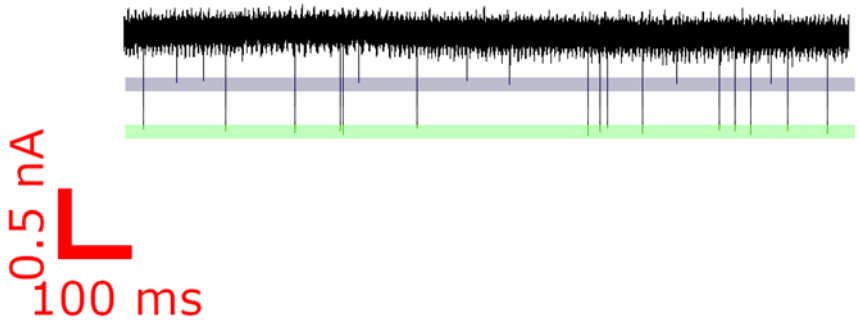

Figure S7. Current–time traces of miRNA and Fe_3O_4-Au-PNA-RNA at +600 mV, with 100 mM KCl containing 10 mM PBS (pH = 7.4).

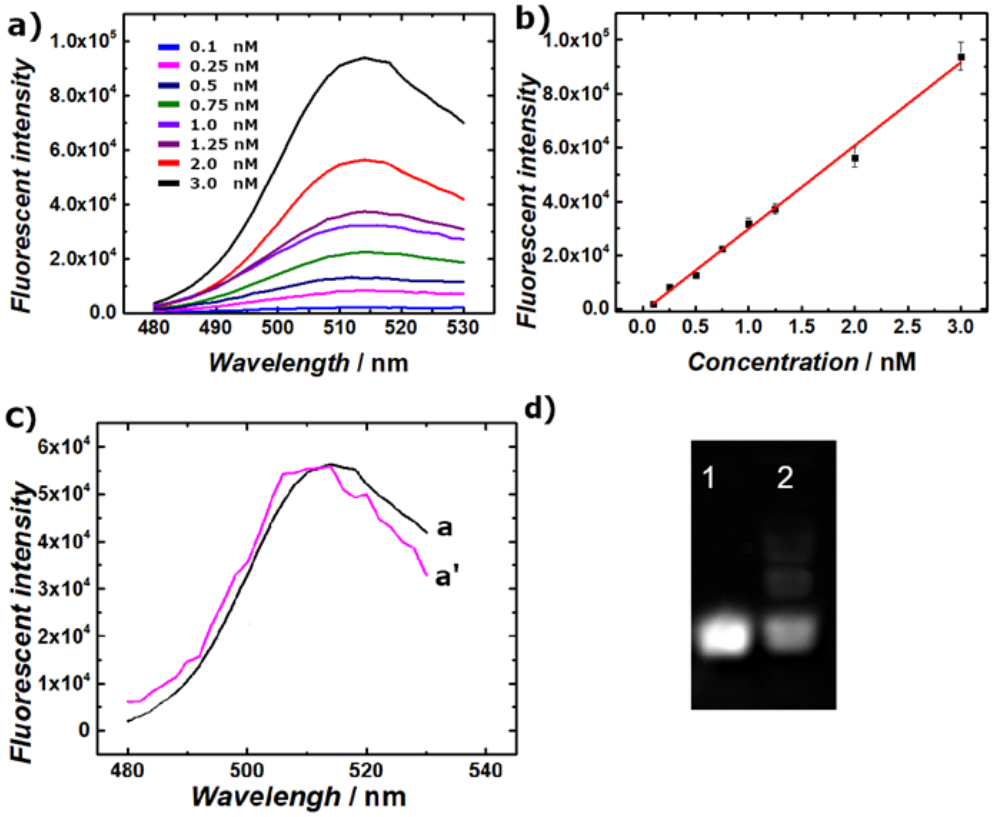

Figure S8. a) Fluorescent spectra of different concentrations of FAM-PNA. b) The standard curve of different concentrations of FAM-PNA. c) Fluorescent spectra of 2nM standard FAM-PNA (curve a) and cleaved FAM-PNA (curve a'). d) Agarose gel electrophoresis of different samples. Lane 1, the ratio of the concentration of NP and PNA were 2:1; Lane 2, the ratio of the concentration of NPs and PNA were 1:1. 2% agarose gel electrophoresis after 90 min @ 100 V in 0.5× TBE buffer.

Carboxyfluorescein (FAM) is a common fluorescent dye with an absorption wavelength of 495 nm and an emission wavelength of 517 nm.[4, 5] First, fluorescent intensity of different concentrations of FAM-PNA was measured to give a standard curve (see **Figure S8a** and **Figure S8b** in Supporting information). After that, FAM-PNAs modified NPs were prepared by the Au-S chemistry, and then the FAM-PNAs on the surface of

NPs were cleaved with DTT by incubating at room temperature for 10 h.[5] Magnetic separation was conducted to separate the free FAM-PNAs from NPs, after which the fluorescent intensity of cleaved FAM-PNAs was measured (see **Figure S8c** in Supporting information**. Curve *a*** was obtained by added 2 nM standard FAM-PNA, while **curve a'** was measured by cleaved FAM-PNA). The number of PNA per NP was calculated as 0.5 by dividing the concentration of the cleaved FAM-PNA determined from the fluorescence measurement to the concentration of NPs, indicating that the NPs had on average either 0 or 1 PNA bound.

We also used gel electrophoresis to determine if the aptamer connection is uniform. The PNA-NP was prepared according to the Au-S chemistry, and the ratio of PNA:NP was 1:2 and 1:1, respectively. After magnetic separation, the excessive miRNA was added and incubated, and after 1.5 hours, the Fe_3O_4-Au-PNA-miRNA were separated by a magnet and washed with the 20 mM Tris-HCl (pH 7.4) containing 150 mM NaCl for several times. These NPs were then reconstituted into a 5 μM solution (calculated by the amount of PNA) for agarose gel electrophoresis. The result was shown in **Figure S8 d**, and the ratios of NP and PNA were 2:1 and 1:1 from left to right, respectively. From **Figure S8d**, it can be observed that there has only one strip from **Lane 1** when the concentration ratio of NP and PNA is 2:1, but have three strips from **Lane 2** when the ratio is 1:1. The first strip in **Lane 2** was on the same level as the strip shown in **Lane 1,** indicating that only one PNA bound with Au nanoparticle when the concentration ratio of NP and PNA is 2:1. However, since more PNAs were added, one Au NP was likely to bound more than one PNA.

In summary, through the fluorescent analysis and gel electrophoresis, our approach ensures that nanoparticle is connected to only one PNA. However, NPs bound 2 or more PNAs still existed and caused obvious long dwell time events (see **Figure S9** in Supporting information). Such events are rare by statistic data analyzing. The vast majority of NPs are just 0 or 1 PNA bonded and the remaining NPs is scarce and does not affect the conclusion.

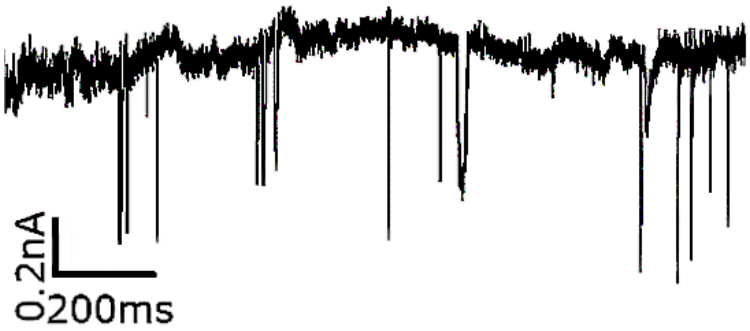

Figure S9. Current-time trace of Fe_3O_4-Au-PNA-RNA on the potential of +600 mV, with some events exhibiting long dwell time.

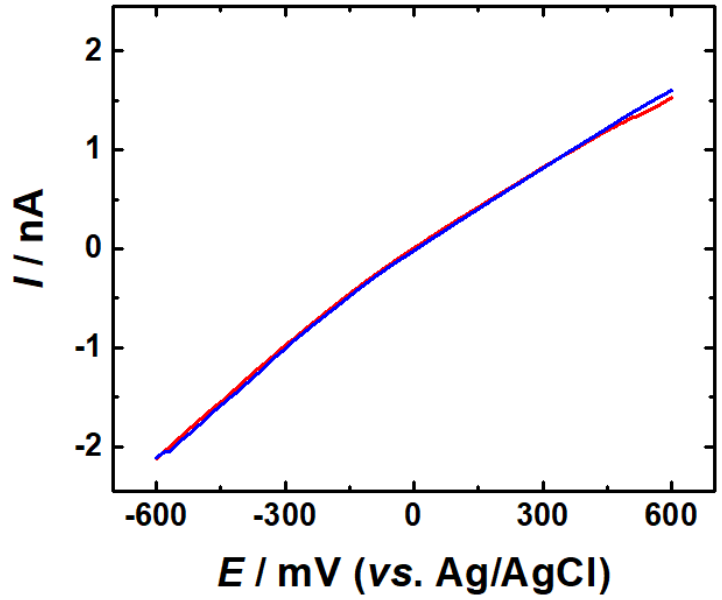

Figure S10. Current-voltage curves of the nanopipette before (blue) and after (red) the translocation experiment. There was little variation, indicating minimal of any analyte adsorption to the nanopore surface.

References

1. Robinson, I.; Tung, L. D.; Maenosono, S.; Wälti, C.; Thanh, N. T., Synthesis of core-shell gold coated magnetic nanoparticles and their interaction with thiolated DNA. *Nanoscale* **2010,** *2* (12), 2624-2630.

2. Freitas, M.; Sá Couto, M.; Barroso, M. F. t.; Pereira, C.; de-los-Santos-Álvarez, N.; Miranda-Ordieres, A. J.; Lobo-Castañón, M. J. s.; Delerue-Matos, C., Highly monodisperse Fe3O4@ Au superparamagnetic nanoparticles as reproducible platform for genosensing genetically modified organisms. *Acs Sensors* **2016,** *1* (8), 1044-1053.

3. Zhao, Y.; Zhang, W.; Lin, Y.; Du, D., The vital function of Fe 3 O 4@ Au nanocomposites for hydrolase biosensor design and its application in detection of methyl parathion. *Nanoscale* **2013,** *5* (3), 1121-1126.

4. Lin, X.; Ivanov, A. P.; Edel, J. B., Selective single molecule nanopore sensing of proteins using DNA aptamer-functionalised gold nanoparticles. *Chemical science* **2017,** *8* (5), 3905-3912.

5. Hurst, S. J.; Lytton-Jean, A. K. R.; Mirkin, C. A., Maximizing DNA loading on a range of gold nanoparticle sizes. *Anal. Chem.* **2006,** *78* (24), 8313-8318.